Extracting winter North Atlantic Oscillation information from a central European stalagmite

Gilliatt, Sam Matthew Rupar

Extracting winter North Atlantic Oscillation information from a central European stalagmite

Sam Matthew Rupar Gilliatt

Department of Earth Sciences

Durham University

December 2012

A thesis submitted for the degree of Master of Science

Abstract

This study explores the potential for extracting winter North Atlantic Oscillation (NAO) information from central European stalagmites using a high resolution calcite $\delta^{18}O$ ($\delta^{18}O_{cal}$) time-series from a stalagmite (AH1) extracted from Atta cave in northwestern Germany. Samples milled at 25µm resolution were run through an isotope-ratio mass spectrometer in weight order. This highlighted the benefit of using a random sample order during isotope ratio analysis because drifts were identified with greater certainty than if the samples were run sequentially. The chronology, constructed using annual $\delta^{18}O_{cal}$ cycles and verified by locating the radiocarbon bomb spike, hints that three isotope excursions may be related to events in the cave history: i) the discovery of AH1 cave passageway in 1985, ii) surface modification during World War Two and iii) the opening of the cave's artificial cave entrance in 1920. However, it was not possible to locate old aerial photographs of the site and appropriate historical documentation, therefore these explanations remain speculative. A good visual correlation between $\delta^{18}O_{cal}$ and meteoric precipitation $\delta^{18}O$ ($\delta^{18}O_{pr}$) cycles was established within the errors of the chronology, but a good quantitative correlation was not achievable probably because the winter $\delta^{18}O_{pr}$ signal was documented by too few $\delta^{18}O_{cal}$ datapoints. Despite the poor quantitative correlation, the good visual $\delta^{18}O_{cal}$- $\delta^{18}O_{pr}$ correlation suggests an annual winter NAO reconstruction is possible using stalagmites from central Europe if ultra high temporal resolution is achieved and excellent chronological control is established. Additionally, this suggests that AH1 is amenable to detection of prolonged shifts in mean NAO state, provided trends associated with other processes are removed.

Table of Contents

Table of Figures

List of Abbreviations

AMOC	Atlantic Meridional Overturning Circulation
ENSO	El Niño Southern Oscillation
IRMS	Isotope ratio mass spectrometer
LIA	Little Ice Age
MWP	Medieval Warm Period
NAO	North Atlantic Oscillation
OT	Original track
TRT	Tip re-mill track
WWII	World War Two
$\delta^{13}C_{cal}$	Calcite $\delta^{13}C$
$\delta^{18}O_{cal}$	Calcite $\delta^{18}O$
$\delta^{18}O_{dw}$	Drip water $\delta^{18}O$
$\delta^{18}O_{pr}$	Meteoric precipitation $\delta^{18}O$

Declaration

This thesis is my own work, except where acknowledgement is made in the text, and is not substantially the same as any work that has been, or is being, submitted to any other university for any degree, diploma or other qualification.

Statement of copyright

Acknowledgements

My thanks go to James, Colin, Lisa, Jo and Jens for their help throughout the project. I also thank DURFC for help in funding my masters and providing a healthy distraction from work. Finally thanks go to my family and friends (particularly those acquainted with Casa Rosa) for their continued support.

1 Introduction

The North Atlantic Oscillation (NAO) is the dominant mode of inter-annual atmospheric variability in the Northern Hemisphere. It controls the strength and position of the mid-Atlantic westerlies and therefore greatly affects European weather and climate [Hurrell (1995)]. The instrumental record for the NAO index, which is defined as the pressure difference between the Azores High and the Icelandic Low, runs from 1821 to present and exhibits several long term trends and reversals [Jones et al. (1997)]. Because this record is relatively short it prevents evaluation of low frequency (decadal to centennial) NAO behaviour and still longer term reconstructions are required. The most recent reversal to a dominantly positive phase since the 1970s is correlated with a rise in global mean temperature [Jones et al. (1997)]. Understanding whether this trend is natural variability or induced by anthropogenic climate change is a critical question for the global climate community [Hurrell et al. (2003)].

Proxy-based reconstructions using tree rings [Cook et al. (1998)], ice cores [Meeker and Mayewski (2002)], corals [Goodkin et al. (2008)], documentary data [Luterbacher et al. (2002)] and multiproxy records [Trouet et al. (2009), Glueck and Stockton et al. (2001), Cook et al. (2002)] have attempted to gain a long term perspective of the NAO. Although these proxy-based NAO indices have revealed prolonged periods of positive and negative NAO modes over the past few centuries, they are often contradictory and still longer term reconstructions are needed.

For example, Trouet et al. (2009) used speleothem and tree ring growth rate as proxies for precipitation amount in Scotland and Morocco respectively, two regions strongly influenced by the NAO. By combining both records, a calibrated NAO reconstruction over the 20th century was constructed and extended to 1050 CE. Their findings suggest a

dominantly positive NAO phase throughout the Medieval Warm Period (MWP; ca, 1000-1300 CE) switched to a more negative phase during the Little Ice Age (LIA; ca 1400-1800 CE). However, this is at odds with previous work by Meeker and Mayewski (2002) who used a sea salt sodium record from the GISP2 ice core to show increased storm frequency during the Little Ice Age, which is indicative of a more positive NAO index.

Trouet et al. (2011) reconcile these two contradicting records by suggesting Meeker and Mayewski's record documents storm intensity rather than frequency, which is consistent with a more negative NAO [Raible et al. (2007)]. This interpretation is dependent on increased Atlantic Meridional Overturning Circulation (AMOC) and a dominant La Niña mode in the Pacific during the MWP that switches to reduced AMOC and dominant El Niño mode during the LIA. Although several studies are consistent with this suggestion, Yan et al. (2011) recently reconstructed a Southern Oscillation index using precipitation proxies from regions that experience significant El Niño Southern Oscillation (ENSO) variability, and found a persistent El Niño like state in the Pacific during the MWP. These conflicting proxy records indicate that more robust reconstructions of both ENSO and NAO variability are necessary to understand climate over the past two millennia.

Although the summer and annual NAO indices are important, the variability of the winter NAO index produces the most atmospheric and climatic variability and also acts as a reasonable proxy for the annual NAO index. This is aptly illustrated by unprecedentedly cold winters of the 2009/2010 and 2010/2011 in western Europe, both of which were caused by extremely negative NAO indices [Seager et al. (2010), D'Arrigo et al. (2011)].

Baldini et al. (2008) demonstrated that December, January, February and March (DJFM) meteoric precipitation $\delta^{18}O$ ($\delta^{18}O_{pr}$) in central Europe exhibits a strong positive correlation with the winter NAO index, and a follow up modelling study by Langebroek et al. (2011) verified these results. Stalagmites are well established proxies of $\delta^{18}O_{pr}$, so stalagmites located within the NAO-$\delta^{18}O_{pr}$ correlation focus offer a unique opportunity to reconstruct the winter NAO beyond the instrumental period, provided a robust chronology is established and the hydrochemistry of the drip feeding the stalagmite is sensitive to annual $\delta^{18}O_{pr}$ fluctuations. This paper aims to determine whether this is possible using a stalagmite (AH1) from Atta cave, northwestern Germany, a location within the focus of the NAO-$\delta^{18}O_{pr}$ positive correlation [Baldini et al., 2008].

Previous studies examining AH1 suggest elevated calcite $\delta^{18}O$ ($\delta^{18}O_{cal}$) values correspond with increased atmospheric production of ^{14}C, which is widely regarded as a solar proxy with higher activities indicative of reduced solar activity and increased cosmic ray flux [Shindell et al. (2001), Niggemann et al. (2003), Jackson et al. (2008)]. Assuming an atmospheric amplification of the Sun's output and that kinetic fractionation controlled $\delta^{18}O_{cal}$, this was interpreted as showing that decreased solar irradiance forced a more negative NAO phase, causing reduced winter rainfall in central Europe, increased kinetic fractionation in AH1, and higher $\delta^{18}O_{cal}$ values. This interpretation was hypothesised using $\delta^{18}O_{cal}$ data sampled at 1500µm resolution where growth rate was ~100µm/a, so any annual $\delta^{18}O_{pr}$ signal was averaged. Using extremely high resolution micromilling (25µm), numerous Hendy tests, and meteoric precipitation and drip water isotope data, this paper aims to determine whether annual cycles in $\delta^{18}O_{cal}$ caused by annual $\delta^{18}O_{pr}$ patterns are present in AH1, and therefore if reconstruction of annual winter NAO indices through time is possible.

2 Material and Methods

2.1 Cave site, history and local climate conditions

2.1.1 Location

Atta cave (57º 07' N, 7º 54' E, elevation ~ 270m) is one of the largest caves in western Germany (Figure 1) with a total passage length of 6700m. The cave system lies in middle Devonian massive limestone deposits underneath the 308m high Sturzenberg, located to the east of Attendorn (Figure 2). The extensively studied Bunker cave [Niggemann et al. (2003a) Riechelmann et al. (2011)] lies ~ 30km to the north west of Atta cave.

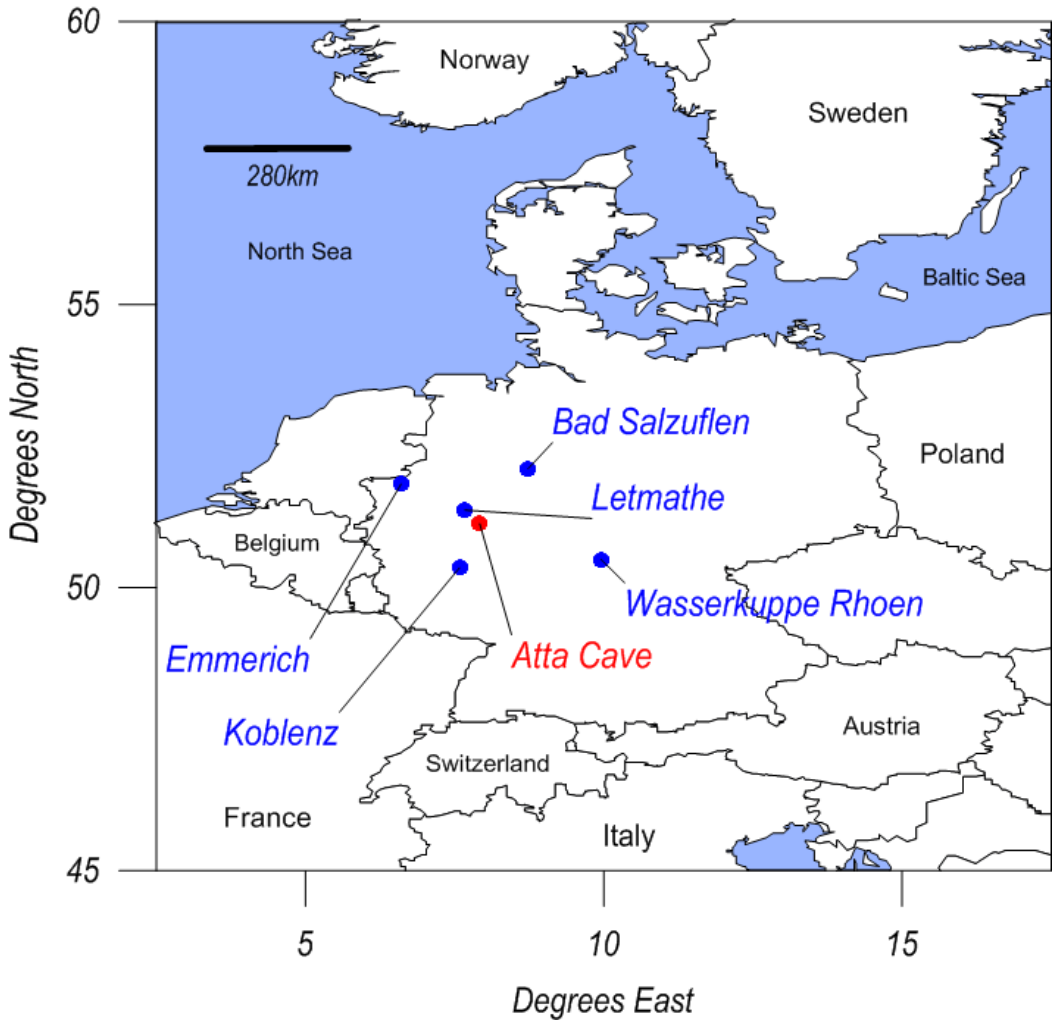

Figure 1 *– Map of western Europe with GNIP data sites and cave location marked.*

2.1.2 History and sample

Around 500m of passages in Atta cave were discovered during mining works in 1907 and guided tours have been taken around this section of cave since its discovery. In 1925, the original entrance was deemed unfit for public use and was subsequently closed after a new artificial entrance was formed. A team lead by Elmar Hammerschmidt discovered the remaining cave passages in 1985 [Jens Fohlmeister personal communication] (Figure 2).

Stalagmite AH1was extracted in 1998 from a 5m high fault orientated cave gallery, 3m above the modern water table. AH1 was located 50m below the surface and 100m away from both the original and artificial cave entrances, and its location represented the

Figure 2 *- Google earth image of ground surface above Atta cave with an annotated cave map overlay. Scale bar is 100m.*

climate of a deep cave (98% humidity and a constant temperature of 9.4ºC). A small soda straw fed AH1 and no interruption to dripping was observed during a 10 month monitoring campaign (March 1997- January 1998). Despite AH1's cave gallery leading to the eastern part of the cave, no air flow was detected in the passageway. A more detailed description of AH1's location is found in Niggemann et al. (2003).

AH1 was previously dated using 18 U-Th points, four of which were measured after Niggemann et al. (2003), with the youngest located 20mm from the tip with a corrected age of 869 BP (dates are given relative to 2000 CE). The average growth rate using all U-Th points is ~75µm/a, with a higher than average growth rate (~100µm/a) from 5550-1660 BP and a lower than average growth rate (~25µm/a) from 1660 BP to AH1's extraction.

2.1.3 Local climate conditions

From 2003 to 2010 mean annual temperature and annual precipitation amount 12 km south east of the cave location (Olpe, Germany) were 9.1ºC and 1172mm, respectively [meteomedia]. The NAO influences weather in Atta cave's vicinity by displacing the mid-Atlantic westerlies north and south depending on its phase. During NAO positive phases, an increased atmospheric pressure gradient between the Icelandic Low and the Azores High enhances Atlantic westerlies, which carry warm and moist maritime air over the Eurasian continent, and causes a northward shift of Atlantic storm tracks. This results in warmer wetter weather in the vicinity of Atta cave. During a negative NAO phase, the pressure gradient between Azores and Iceland is reduced resulting in weaker westerlies and a southward shift in Atlantic storm tracks. This displaces the warm, wet weather towards the Mediterranean [Hurrell (1995)], resulting in colder and drier conditions around Atta cave.

2.2 Precipitation and drip water isotope data

Four GNIP data sites within 160km of Atta cave were used throughout the study: Bad Salzuflen (120km), Wasserkuppe Rhoen (160 km), Koblenz (90km) and Emmerich (140km) (Figure 1). To avoid a bias towards any one of these stations, contemporaneous data (1978-2007) from all four sites was averaged. Precipitation isotope data taken from Letmathe (30km) and AH1 drip water isotope data were also utilised from Stefan Niggeman's PhD thesis [Niggemann (2000)].

2.3 Micromilling

Fairchild et al. (2006) suggested the preferred method for obtaining stalagmite stable isotope time-series data is to sample the stalagmite carbonate down the growth axis using an automated micromill. Following this, the milled powder is digested by orthophosphoric acid to produce CO_2 which is analyzed by an isotope-ratio mass spectrometer (IRMS). Typically analysis is undertaken by running the samples through the IRMS sequentially (i.e. in the order they are milled from the stalagmite) because often this is the most straight forward method. In testing AH1's suitability to reconstruct annual winter NAO indices, this study also examines a refinement of this method which involves running the samples in weight order, rather than sequentially.

Assuming an average growth rate of ~100µm/a over the instrumental period, which is broadly consistent with the U-Th chronology and is typical of temperate zone stalagmites, the original track (OT) was milled down AH1's central growth axis using a ESI/New Wave micromill at 50µm intervals (biannual resolution based on 100µm/a growth rate) to produce powders for stable isotope analysis (Figure 3). Ideally, the depth and width of the OT would be determined using the method outlined by Fairchild et al. (2006). However, AH1 lacks laminations, so the depth (200µm) and width (2500µm) of

the OT were determined iteratively using calcite's density of 2.81g/cm^3 to give sample weights >45µg using a 50µm milling interval.

After milling 77 samples at 50µm intervals, sufficient powder production allowed an increase in resolution to 25µm intervals (seasonal resolution based on a 100µm/a growth rate). This resolution was continued to 19,850µm from the AH1's tip (the end of the NAO instrumental period, based on a growth rate of 100µm/a). Beyond this, a 50µm resolution was continued to 22,300µm, giving a total of 760 samples in 22.3mm (Figure 3).

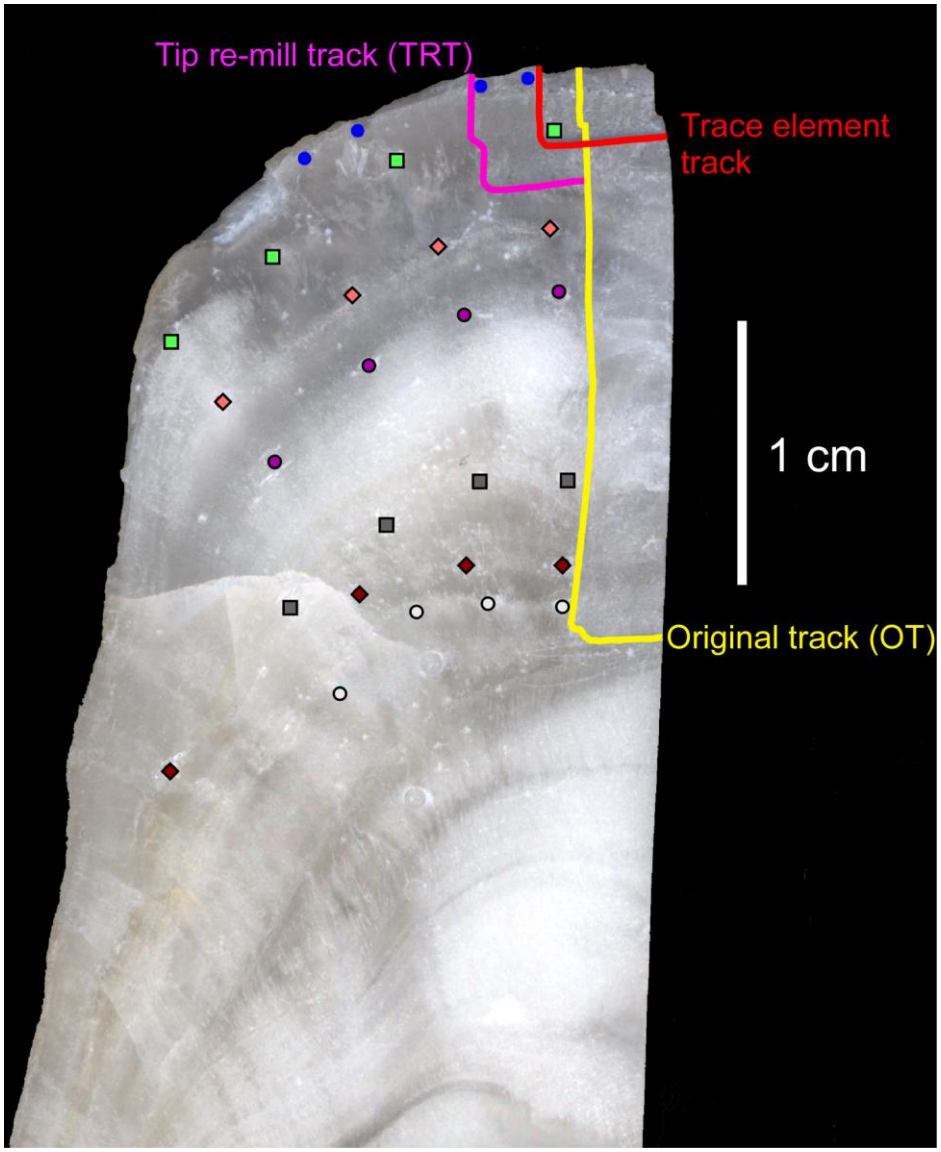

Figure 3 *- Scan of AH1's tip with the location of all milling tracks and Hendy test pits marked.*

To ensure the same resolution throughout the entire NAO instrumental period and to test the reproducibility of the OT, 182 samples were milled from AH1's tip at a 25µm resolution parallel to the OT. The tip re-mill track (TRT) was milled 1,000µm wider than the OT to yield increased sample weights for analysis (Figure 3).

Trace element powders were milled at 100µm intervals from AH1's tip to 3100µm to test a hypothesis regarding the nature of an isotope excursion at 1550µm (see discussion and Figure 3). The trace element track was milled over the OT and TRT so was milled from a depth of 200µm to 400µm.

2.4 Hendy Tests

Seven Hendy Tests were conducted, each one containing four sampling points. Ideally these samples would come from the same visible lamella for each Hendy Test [Hendy (1971)]. However, AH1 does not contain annual laminations so petrographic horizons were used as guides instead (Figure 3).

2.5 Isotope Analysis

Milled powders, varying in weight from 42 to 210µg, were transferred to 4.5ml Labco exetainer vials for stable carbon and oxygen isotope analysis. Many previous studies have used larger 12ml vials for isotope analysis, but following the technique outlined by Brietenbach and Bernasconi (2011), 4.5ml vials were used which allowed accurate and precise measurement of smaller sample weights and a higher micromilling resolution.

To keep sample weights similar to the standards used to correct them, all samples from the OT were weight ordered (heaviest first) and run through Durham University's Thermo-Finnigan MAT 253 IRMS online with a Gasbench II. Typically, batches of 44 samples were interspersed with standards every 14 or 15 samples, with a total of four

sets in each batch. International standards NBS18, NBS19 and LSVEC were used for calibration. Initially drifts were evaluated using the Durham University in house standard DCSO1 by calculating the difference between the first and last DCSO1 in the batch, dividing by the total number of analysis, and multiplying this value by the samples', or standards', position in the batch. Drifts were only applied where it was obvious all the standard values were drifting throughout a batch. If the drift correction improved the standard deviation of the batches' standards, it was regarded as correct. However, there was often ambiguity as to whether drift corrections should be applied. For example, in several instances applying a drift correction improved some standard deviations whilst others deteriorated. In these cases, the decision on whether to apply a drift correction or not was made based on the standards closest in value to the samples, and the behaviour of the samples themselves through a run. Drift corrections are discussed in more detail in the results and discussion below.

3 Results and discussion

3.1 Drift Corrections

Before interpreting the OT data with respect to climate, the dataset was examined for possible analytical artefacts. Running the milled samples in weight order offered a unique opportunity to do this, because a given sample's chemistry should be completely independent of the preceding and succeeding samples in terms of climate processes.

When the $\delta^{18}O_{cal}$ data is plotted in weight order, cycles with amplitudes of ~0.5 to 0.75‰ and varying wavelength are evident (Figure 4a). These 'cycles' are explained by a secondary level of sorting, dependent on distance from AH1's tip, that was inadvertently applied when the samples were placed in weight order. Each cycle represents one sample weight and the cycle geometry illustrates a 'snapshot' of the overall dataset's morphology, i.e. elevated values during the middle section of the time-series and generally lower values at the beginning and the end. Note that these cycles are also evident in the OT calcite $\delta^{13}C$ ($\delta^{13}C_{cal}$) data and the same explanation applies.

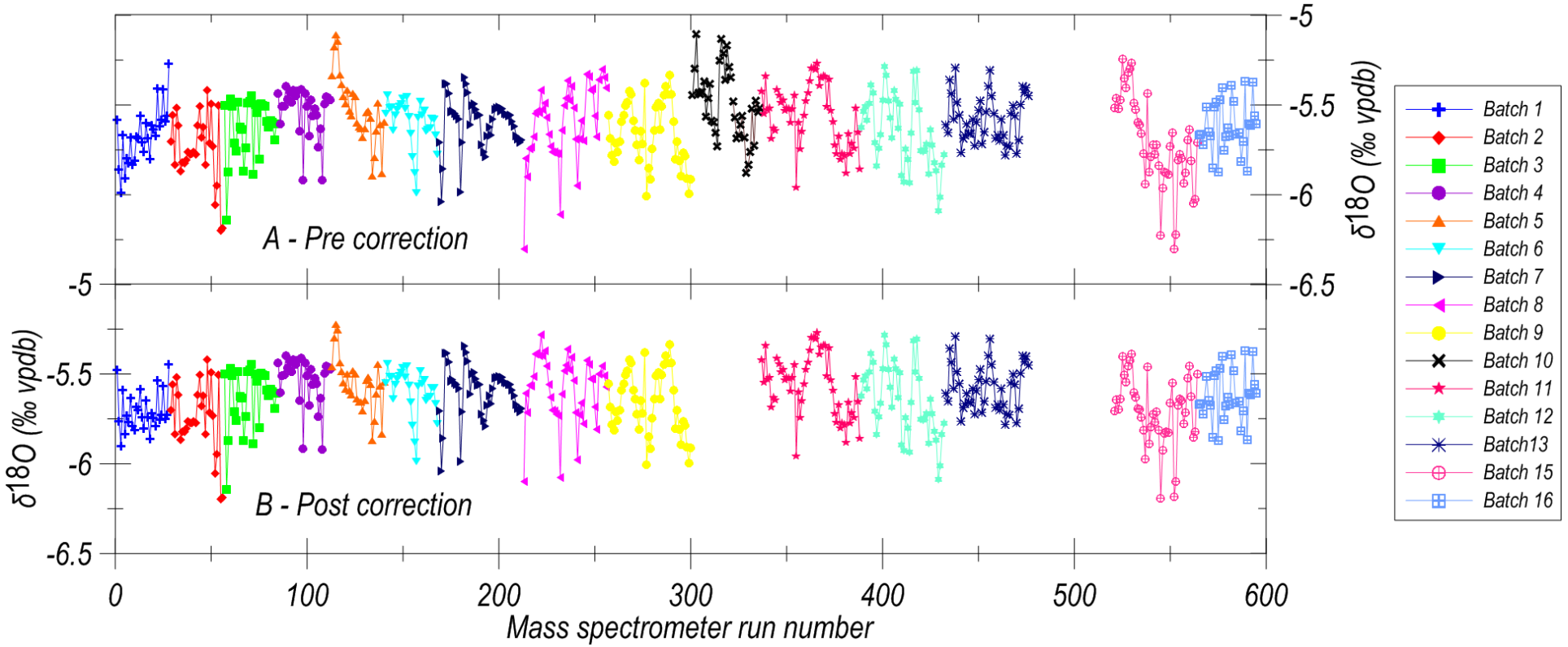

Figure 4a *– Pre (A) and post (B) correction OT $\delta^{18}O_{cal}$ data plotted as batches relative to the mass spectrometer run number.*

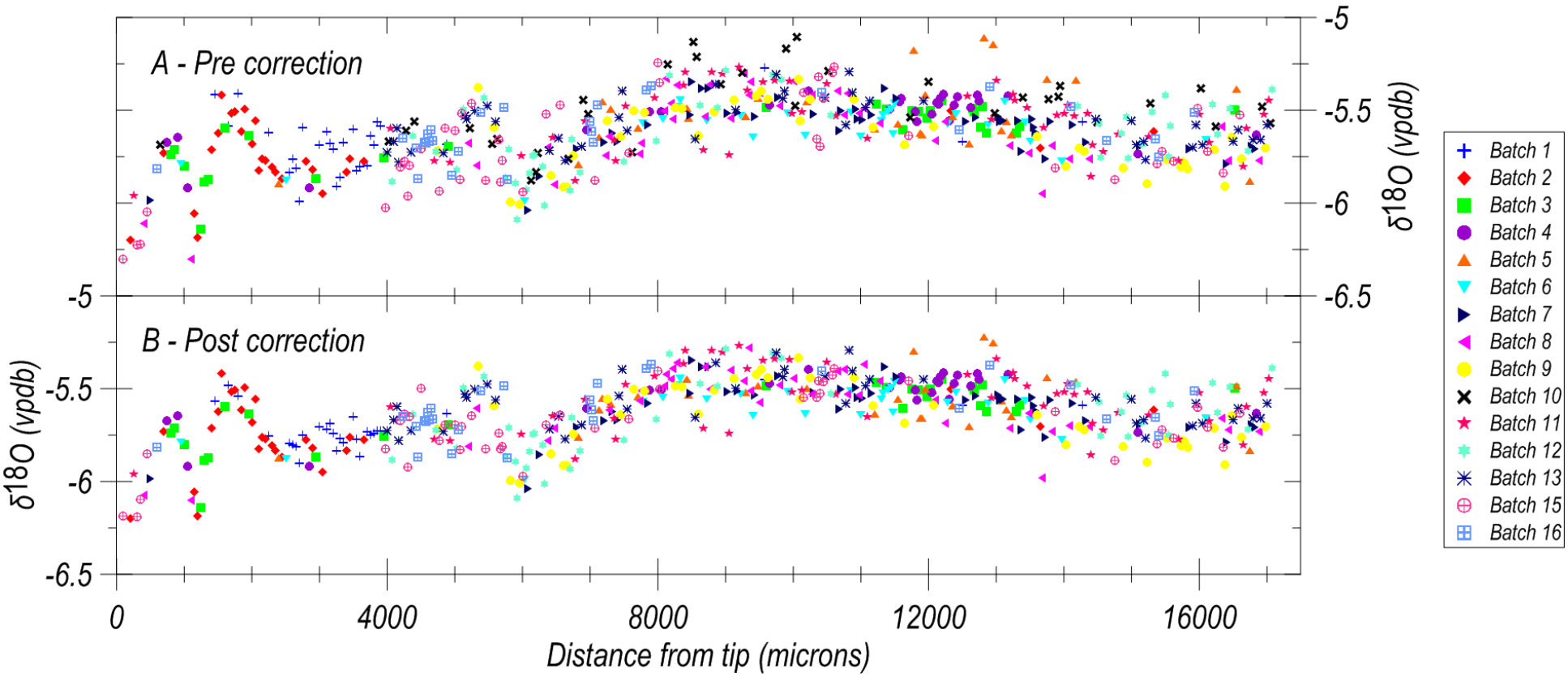

Figure 4b *– Pre (A) and post (B) correction OT* $\delta^{18}O_{cal}$ *data plotted as batches relative to the distance from AH1's tip.*

In contrast to the cycles present in most batches, the overall positive or negative gradient evident in batches one, five, eight, ten and fifteen's $\delta^{18}O_{cal}$ data was genuinely concerning (Figure 4a). Unidentified drifts, or erroneously applied drifts, are the likely cause of the monotonic increase, or decrease, in $\delta^{18}O_{cal}$ values across these batches. Fortunately, these artefacts were identified and corrected for (Figures 4a and 4b), but this was only possible because the samples were run in weight order; had the samples been run in sequential depth order, the artefacts would possibly have remained unidentified. Noise in the standards' values, used to check if applied drift corrections were correct, is the likely cause of these unidentified, or in some cases erroneously applied, drifts.

Note that these unidentified, or incorrectly applied, drifts were not evident in the $\delta^{13}C_{cal}$ data. However, for consistency's sake, $\delta^{13}C_{cal}$ and $\delta^{18}O_{cal}$ data from the same batch were always corrected in the same way, using the $\delta^{13}C$ values of the relevant standards.

Where drift corrections were added or removed in this phase of analysis, standard deviations were always improved or partially improved (i.e. at least two of the four standards' standard deviations were improved).

It was possible to correct the data from batches one, five, eight and fifteen (Figures 4a and 4b) but unfortunately it was not possible to justifiably improve the drift evident in batch ten. To improve this data, a drift in the opposite direction to the drift evident in batch ten's standards was necessary. Therefore this batch was deemed untrustworthy and has not been included in any of the data that follows. Unfortunately the data from batch 14 were also lost due to a fault with the laboratory computer.

The same batch evaluation process was undertaken for the TRT samples, which were run in weight order separately to the OT samples. Maximum errors for both the OT and TRT $\delta^{18}O_{cal}$ and $\delta^{13}C_{cal}$ values were 0.1‰.

Running the samples in weight order allowed an important secondary check on the batches' drifts to be undertaken. However, because a secondary level of sorting was inadvertently applied when putting the samples in weight order, there was some link in chemistry between the adjacent samples and therefore some uncertainty was imparted to the evaluation. If this secondary level of sorting was avoided, i.e. if the samples had been randomised prior to analysis, the cycles mentioned previously would not be evident and the drifts could be evaluated with even more certainty.

3.2 Preliminary Observations

$\delta^{18}O_{cal}$ in the OT varies from -6.38‰ to -5.22‰ (VPDB), with an mean value of -5.65‰ (Figure 5). Starting furthest from the stalagmite's tip (or furthest back in time), the $\delta^{18}O_{cal}$ generally increases from -6.25‰ at 22,300µm to -5.45‰ at 8,000µm. Following this, a pronounced decrease in values to -6‰ at 6,000µm and a sharp increase to -5.5‰ at 5,300 occurs. The final 5,000µm are characterised by generally decreasing values but with the most pronounced excursion of the dataset occurring at 1,550µm with a magnitude of 1.5‰. Throughout the 25µm resolution dataset small scale cycles are superimposed on top of the large scale isotope excursions (Figure 5).

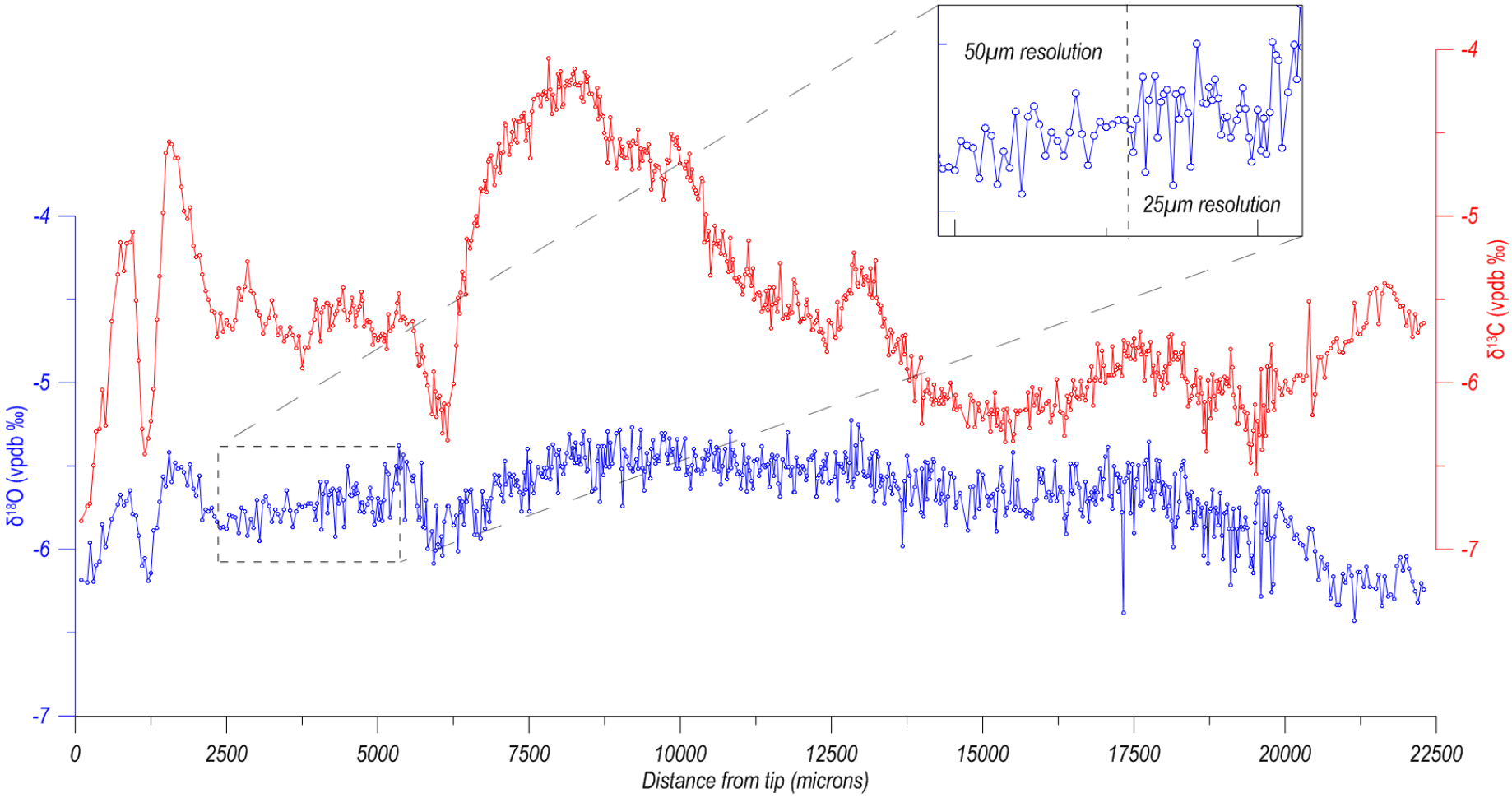

Figure 5 *- OT $\delta^{18}O_{cal}$ and $\delta^{13}C_{cal}$ time-series plotted on a depth scale. The boxed region marks the transition from 50µm to 25µm milling resolution.*

The cycles present in the OT $\delta^{18}O_{cal}$ data milled at 25µm do not appear in the data milled at 50µm (Figure 5). This illustrates the value of micromilling at high resolution and that large milling intervals can result in overlooked information. Due to low sampling resolution, many previous stalagmite climate records have not detected seasonal climate fluctuations, and therefore were not able to use this information to help interpret long term (decadal to millennial scale) geochemical shifts. However, this information could prove invaluable for understanding these records because parameters that influence stalagmite geochemical proxies on longer time scales are probably an extension of seasonal influences.

The $\delta^{13}C_{cal}$ OT data follows a similar trend as the $\delta^{18}O_{cal}$ OT data, but with more pronounced excursions of higher magnitude. Unlike the other $\delta^{13}C_{cal}$ excursions which occur synchronously with $\delta^{18}O_{cal}$ events, the increase in $\delta^{18}O_{cal}$ values at 5300µm is preceded by an increase in $\delta^{13}C_{cal}$ by ~200µm. Small scale cycles are also evident in the in $\delta^{13}C_{cal}$ data but are poorly defined.

3.3 Tip re-mill tuning

Plotting the TRT data against the OT data highlights some ‘compression’ in the tip re-mill dataset (Figure 6, panel A). These findings are similar to those of Fairchild et al. (2006) and were expected because stalagmite lamination thickness decreases with distance from the growth axis. Using key inflection points in both $\delta^{13}C$ datasets (OT and TRT) it was possible to ‘tune’ the TRT’s data point locations to the OT’s depth scale by shifting the location of the inflection points in the TRT data to match the location of the inflection points in the OT (Figure 6). $\delta^{13}C_{cal}$ data was chosen over $\delta^{18}O_{cal}$ for tuning because the isotope excursions are more pronounced and easily identifiable in the $\delta^{13}C_{cal}$ data.

After tuning, the TRT data shows higher $\delta^{13}C_{cal}$ values compared to the OT data, particularly at the positive inflection points located at ~2750 and ~5400µm (Figure 6 panel B). This is discussed in more detail below after introducing the Hendy test results, but most likely results from minor kinetic fractionation as the drip water moves to the flank of the stalagmite. It is worth noting that the temporal resolution of the TRT is lower than an equivalent track milled at the same spatial resolution directly on the growth axis, due to slightly slower growth rate away from the growth axis; however, due to the very small distance from the growth axis to the TRT position, this effect is minimal.

The tuning applied to the $\delta^{13}C_{cal}$ data was also applied to the $\delta^{18}O_{cal}$ data. Having a 25µm resolution covering AH1's tip allowed detection of small scale isotope cycles from AH1's tip continuously to 19,850µm, where the 25µm resolution ended.

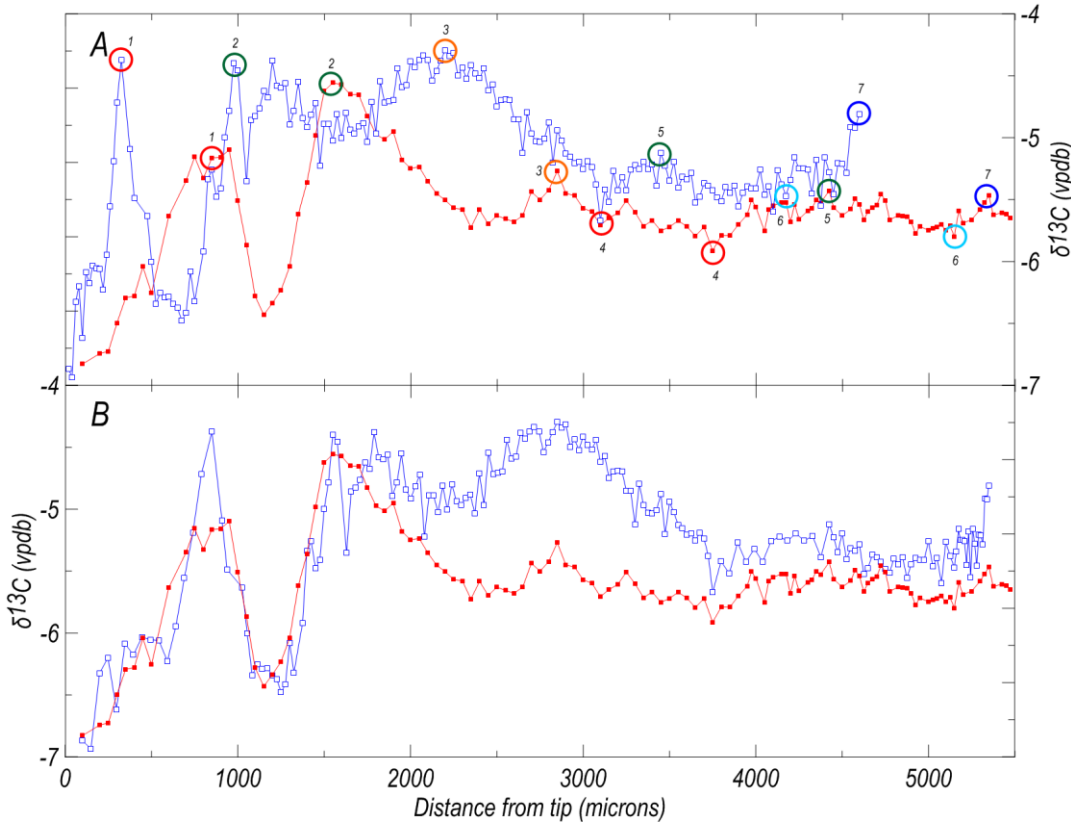

Figure 6 *– Un-tuned (A) and tuned (B) TRT $\delta^{13}C_{cal}$ data (blue) compared to the OT $\delta^{13}C_{cal}$ data (red). All time-series plotted on a depth scale. Circles of the same colour in panel A mark the TRT points that were tuned to the corresponding OT points.*

3.4 Chronology development

3.4.1 Cycle count- are the $\delta^{18}O_{cal}$ cycles annual?

The $\delta^{18}O_{cal}$ cycles have a wavelength of ~105µm which is similar to the annual growth rate implied by the U-Th chronology [Niggeman et al. (2003)] and is typical of a temperate zone stalagmite. Unfortunately, the cycles are poorly developed from the top of the stalagmite to a depth of 1550µm. Therefore, a tentative chronology was constructed by counting $\delta^{18}O_{cal}$ cycles assuming i) the $\delta^{18}O_{cal}$ cycles are annual, and ii) that the discovery of the passage containing AH1 in 1985 (1550µm) somehow disrupted the preservation of well-developed cycles (discussed below). Essentially, peaks were counted back from a depth of 1550µm, assuming this depth corresponds to 1985. Cycle peaks, rather than minima, were used to conduct the cycle count because they are characterised by more datapoints. A cubic smoothed spline was used to convert depth values to time values using the cycle count chronology.

To test the cycle count chronology, the location of AH1's radiocarbon datapoints were plotted using the chronology and compared to the atmospheric bomb spike (Figure 7 on page 21), a method previously used by Mattey et al. (2008) and Genty et al. (1998). Extrapolating AH1's radiocarbon data to produce a hypothetical stalagmite bomb spike suggests there is a six year radiocarbon signal transfer between the atmosphere and AH1. Using this six year lag and the time interval integrated during the sampling of each radiocarbon sample, the atmospheric radiocarbon activity was calculated (Figure 7). The remarkable similarity between the position of the averaged atmospheric radiocarbon datapoints and the AH1 radiocarbon datapoints using the $\delta^{18}O_{cal}$ cycle-based chronology, strongly suggests the assumptions used to produce the chronology are valid and that the chronology is accurate.

Unfortunately, splicing together the overlapping 25µm resolution data in the TRT and OT was not possible because the cycles did not match up. Therefore the cycle count was continued in the OT data at the end of the TRT. Unfortunately, this may have imparted some error into the OT dating beyond the TRT data because the end of the TRT cycle count may not predate the start of the OT cycle count.

A linear growth rate based on the cycle count data was used to construct a chronology for the 50µm resolution OT data milled from 19850µm to 22300µm (covering the pre-instrumental portion of the record) because the cycles are not present in the 50µm data.

3.4.2 Cycle count errors

Four independent cycle counts were conducted (each by a different individual) to check the reproducibility of the chronology and to estimate the errors associated with it. In the original cycle count, covering both the TRT and OT data, 189 cycles were established. Of the three other cycle counts, a maximum and minimum of 217 and 152 cycles were counted respectively. Assuming no error exists at the start of the cycle count (i.e. 1985 is assigned to the correct depth and the first cycle is 1985), this suggests a maximum error of ± 37 years (189 minus 152) at the end of the cycle count chronology. This does not include any error induced by continuing the cycle count in the OT data at the end of the TRT data, despite the inability to 'splice' the two datasets together.

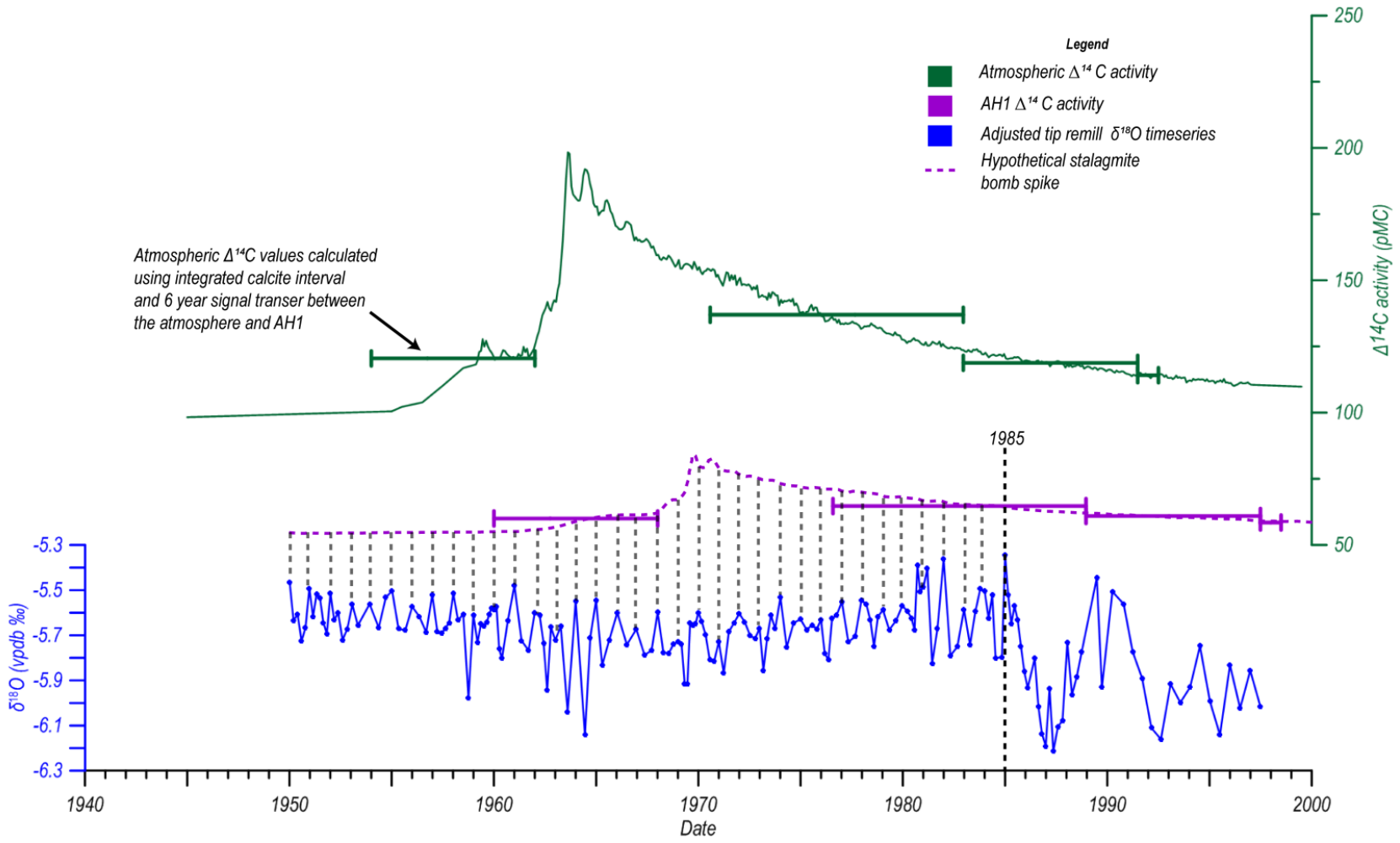

Figure 7 *- AH1 radiocarbon datapoints plotted using the $\delta^{18}O_{cal}$ cycle count chronology (blue) with an extrapolated stalagmite bomb spike marked (purple), compared to the atmospheric bomb spike (green) [Hua and Barbetti (2004), Stuiver et al. (1998)]. Error bars show the integrated calcite interval used to for each radiocarbon point (see text for explanation).*

3.5 Kinetic Fractionation

3.5.1 Hendy tests

Before interpreting the time-series it is important to discuss if kinetic isotope fractionation is influencing AH1's chemistry. Co-variation clearly exists between the $\delta^{13}C_{cal}$- $\delta^{18}O_{cal}$ datasets (Figures 5 and 8), which is sometimes indicative of kinetic fractionation. However, the co-variation may also result from climatic forcing which acts to push both $\delta^{13}C_{cal}$ and $\delta^{18}O_{cal}$ in the same direction [McDerrmott (2004)].

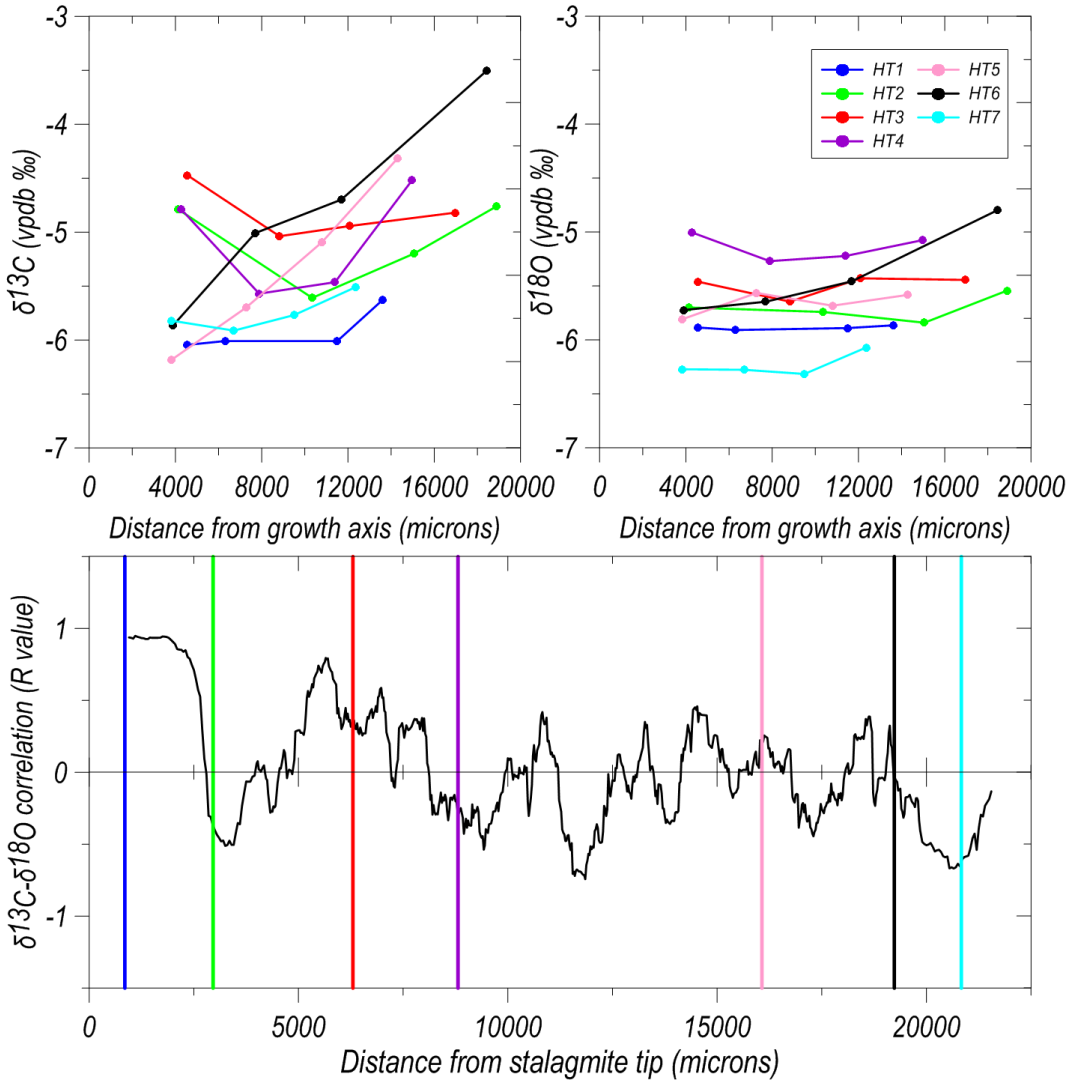

Figure 8 *- $\delta^{13}C_{cal}$ (upper left panel) and $\delta^{18}O_{cal}$ (upper right panel) Hendy test results plotted relative to the distance from AH1's growth axis. The lower panel compares the location of the Hendy tests with the OT $\delta^{13}C_{cal}$ - $\delta^{18}O_{cal}$ time-series correlation.*

Comparing the Hendy test data against the OT $\delta^{13}C_{cal}$- $\delta^{18}O_{cal}$ correlation suggests the latter is true for AH1 (Figure 8). If kinetic fractionation was the causing the co-variation evident in the datasets, periods of high correlation should correspond with a strong positive gradient in a Hendy Test conducted along that horizon, which is not the case.

However, because it is not theoretically possible for isotope ratios to decrease away from the growth axis, only Hendy tests one, six and seven can be viewed with confidence. Incorporation of calcite adjacent to the targeted calcite is the likely explanation for the misleading results in Hendy tests two, three, four and five. With this in mind, only Hendy test six suggests with confidence that kinetic fractionation is taking place.

The Hendy test data suggest that, in general, $\delta^{13}C_{cal}$ increases more than the $\delta^{18}O_{cal}$ away from the growth axis. This is unsurprising because degassing more significantly increases $\delta^{13}C_{cal}$ values than $\delta^{18}O_{cal}$ values, and thus is also the likely explanation for the increased $\delta^{13}C_{cal}$ values in the TRT data relative to the OT (Figure 6). If considerable evaporation was taking place on AH1, significantly increased $\delta^{18}O_{cal}$ values away from the growth axis would be expected, which is not the case when TRT and OT $\delta^{18}O_{cal}$ data are compared, or in the Hendy test data (Figure 8).

3.5.2 Fractionated GNIP data

Using the averaged GNIP data and the fractionation factor derived by Tremaine et al. (2011) based on in-cave observations, the average value of -5.7‰ (VPDB) for the TRT $\delta^{18}O_{cal}$ data is 0.67‰ higher than it should be at isotopic equilibrium when using the annual average cave temperature of 9.4ºC (Figure 9). Utilising the commonly used Kim and O'Neil fractionation factor suggests the average TRT $\delta^{18}O_{cal}$ value is 1.4‰ higher than it should be at isotopic equilibrium [Kim and O'Neil (1997)]. The disparity in

fractionated GNIP data values when using the different fractionation factors occurs because Tremaine's fractionation factor was calculated using natural cave locations where fractionation factors are higher than laboratory derived values, like Kim and O'Neil's. This is consistent with the results presented here because the fractionated GNIP data values are 0.73‰ higher using Tremaine's fractionation factor compared to Kim and O'Neil's.

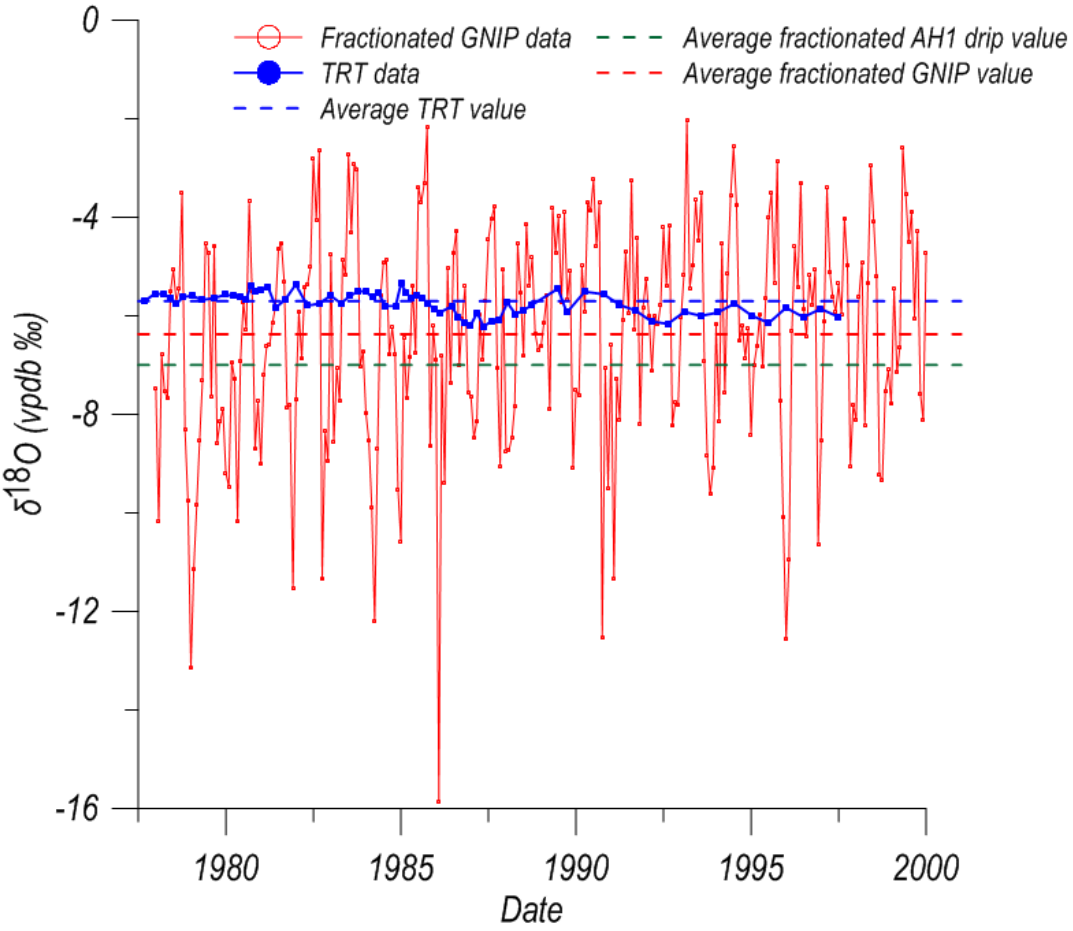

Figure 9 *- TRT $\delta^{18}O_{cal}$ time-series (blue) compared to the fractionated GNIP data time-series (red). Average values are also marked, including the average fractionated value of the AH1 drip data (green). Fractionated values were calculated using the equation developed by Tremaine et al. (2011).*

Kinetic fractionation is one explanation for the increased values when using both fractionation factors but it is also possible that summer evapotranspiration above the cave is acting the raise the isotope ratios before infiltration into the karst. However, the limited AH1 drip data has an average value of -8.92‰ (SMOW) which is 0.69‰ more negative than the average GNIP value (-8.23‰), which suggests isotope values are not being raised prior to karst infiltration. Therefore, kinetic fractionation is probably taking place in to some degree in AH1, but the Hendy test results suggest it is probably not the dominant control on stable isotope ratios of the stalagmite through time.

3.6 Dataset interpretations

3.6.1 Isotope Excursions

3.6.1.1 1550µm: cave exploration

As discussed previously, the cycle count chronology combined with the radiocarbon data strongly suggest the carbon and oxygen isotope excursion at 1550µm was caused by the cave exploration in 1985 (Figures 7). One possibility implicates physical disturbance or contamination by cavers, either directly by touching, or indirectly by generating dust that settled onto the stalagmite. Trace element data obtained from the stalagmite support this interpretation. Lead was detected in abundance between AH1's tip and 1985 (based on the cycle count chronology) but not before (Figure 10), and yttrium and thorium follow a similar trend. This strongly suggests that the contamination is linked to the discovery of AH1's cave passage, possibly related to accidental caver contamination.

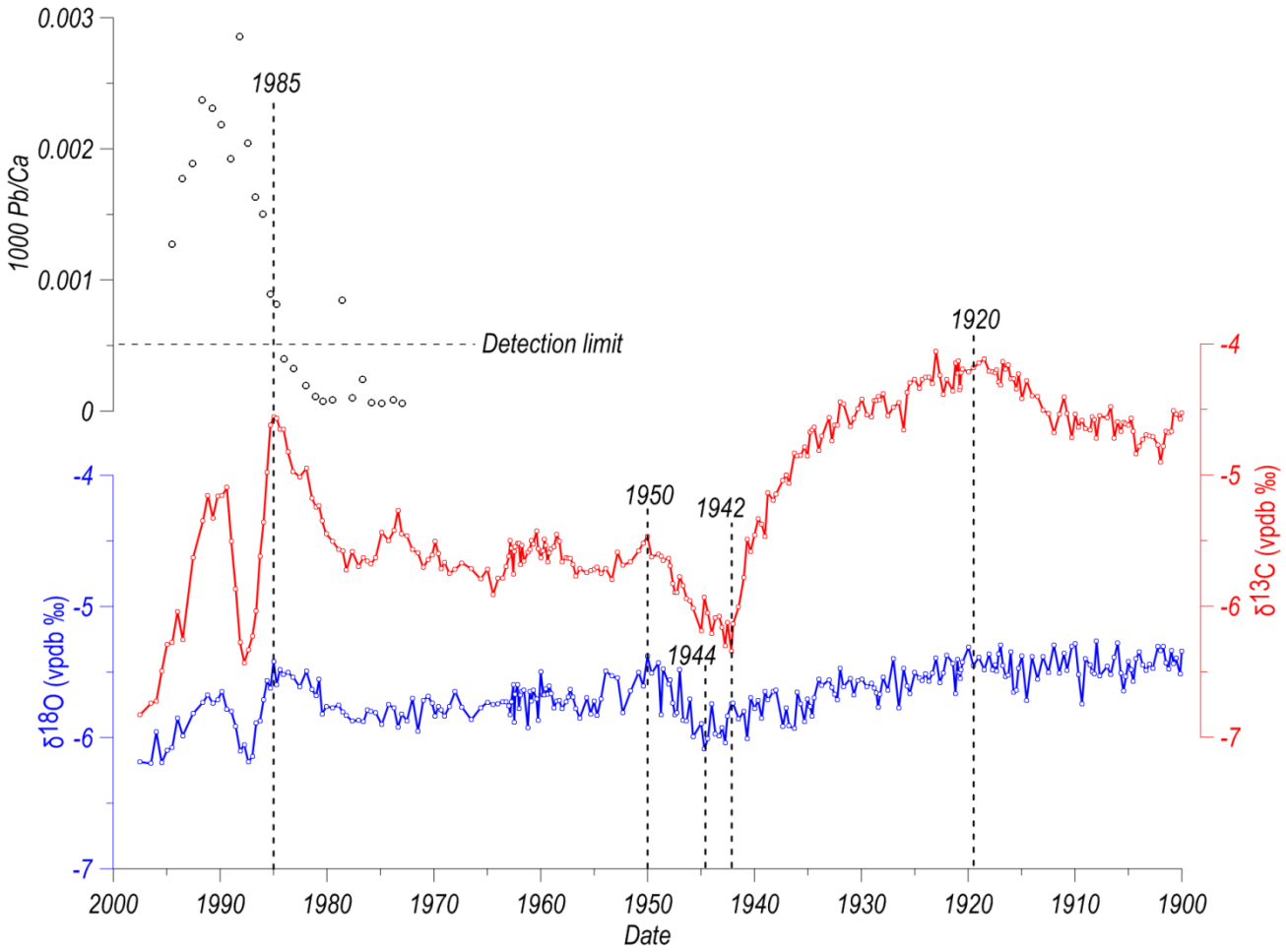

Figure 10 *- OT $\delta^{18}O_{cal}$ (blue) and $\delta^{13}C_{cal}$ (red) time-series over the 20th century with key dates marked. Upper panel shows the Pb/Ca trace element data with the detection limit marked. All data plotted using the cycle count chronology.*

3.6.1.2 6000µm: WWII

Using the cycle count chronology, the $\delta^{13}C_{cal}$ and $\delta^{18}O_{cal}$ excursion ~6000µm from AH1's tip corresponds to a start and end date of 1942 to 1950 and 1944 to 1950 in the $\delta^{13}C_{cal}$ and $\delta^{18}O_{cal}$ data, respectively (Figure 10). Due to the chronological uncertainties, this excursion may reflect World War Two (WWII) in some way. The offset in start date between the carbon and oxygen isotope data, with carbon coming first, hints that the excursions were caused by land use changes. The top of the Sturzenberg above the cave was cleared in the past (Figure 2), and if this clearing occurred during WWII it may have affected the isotope ratios of the stalagmite.

If this is the case, the $\delta^{13}C_{cal}$ values increased in response to a lesser contribution of isotopically light biogenic carbon after the vegetation above the cave was cleared [e.g. Baldini et al. (2005)], whereas the oxygen isotope excursion may have resulted by increased infiltration of isotopically heavier summer rainfall due to less evapotranspiration above the cave after the vegetation clearing took place. To test this hypothesis, the National Collection of Aerial Photography archive in Edinburgh was searched for evidence of vegetation clearing during WWII. However, no records were found, so this hypothesis remains speculative.

3.6.1.3 8000µm: Secondary cave entrance opening?

Decreasing isotope ratios starting at around 8000µm (1920) broadly coincide temporally with the creation of the second cave entrance in 1925 (Figure 10). The five year offset is within the error of the cycle count chronology. However, explaining the decreasing isotope ratios by appealing to the development of the second cave entrance is challenging. Increased ventilation associated with a cave opening would generally increase degassing and result in increased kinetic fractionation and increased isotope

ratios, which is at odds with the decreasing isotope ratios from ~1920. A plausible explanation is that after opening the 1925 entrance, the 1907 entrance was closed which resulted in rerouting of cave air flow away from AH1's location, therefore decreasing degassing, kinetic fractionation and isotope ratios. Niggeman's qualitative observation that no air flow currently occurs in AH1's cave gallery is consistent with this suggestion. However, the date of the primary cave entrance's closure remains unknown and the secondary cave entrance is closer to AH1's location than the primary entrance (Figure 2), so unfortunately this hypothesis remains speculative.

3.6.2 $\delta^{18}O_{cal}$ cycles: do they reflect annual $\delta^{18}O_{pr}$ cycles?

The matching geometry of the AH1's radiocarbon data with the atmospheric radiocarbon points strongly suggests the TRT $\delta^{18}O_{cal}$ cycles are annual (Figure 7). When the TRT cycles are compared to the $\delta^{18}O_{pr}$ GNIP data, it is clear AH1 drip water is extremely well mixed when it reaches the drip site (Figure 9). However, the limited AH1 drip water $\delta^{18}O$ ($\delta^{18}O_{dw)}$ data suggests the drip is fed by dual component flow, because the annual fluctuation in the GNIP $\delta^{18}O_{pr}$ values is still evident in the $\delta^{18}O_{dw}$ (Figure 11).

This observation is consistent with the data presented in Figure 12 (page 30), which illustrates that the $\delta^{18}O_{cal}$ cycles reflect the annual fluctuation in $\delta^{18}O_{pr}$. The $\delta^{18}O_{cal}$ - $\delta^{18}O_{pr}$ correlation was established by shifting the entire $\delta^{18}O_{cal}$ dataset by 1.5 years. Although this part of the TRT data has a low chronological error because it is close to the start of the cycle count, this 1.5 year shift is acceptable because seasons were not considered when undertaking the cycle count or establishing the location of the 1985 excursion.

The $\delta^{18}O_{cal}$ - $\delta^{18}O_{pr}$ visual correlation is remarkably good from 1978 (the start of the GNIP data) to ~ 1986 where the isotope excursion associated with contamination during cave exploration degrades the $\delta^{18}O_{pr}$ signal in the $\delta^{18}O_{cal}$ data. However, some similarity exists in the time-series until ~1992 despite the contamination (Figure 12).

From the start of the GNIP $\delta^{18}O_{pr}$ data (1978) to 1986, where the $\delta^{18}O_{cal}$ - $\delta^{18}O_{pr}$ correlation is degraded, the winter (DJF) $\delta^{18}O_{pr}$ – winter (DJF) NAO index correlation has an R^2 of 0.71. Despite the excellent visual $\delta^{18}O_{cal}$ - $\delta^{18}O_{pr}$ correlation, this R^2 could not be reproduced using the winter $\delta^{18}O_{cal}$ values and winter NAO indices. This is probably because winter $\delta^{18}O_{pr}$ is only reflected by two or fewer datapoints in the $\delta^{18}O_{cal}$ data and the true winter $\delta^{18}O_{pr}$ signal is not reconstructed by averaging these datapoints. To improve this correlation, and therefore the ability to reconstruct annual winter NAO indices using $\delta^{18}O_{cal}$, yet higher resolution records are necessary. However, annual reconstruction of winter NAO indices is very ambitious and longer scale reconstructions are more realistic. The good visual $\delta^{18}O_{cal}$ - $\delta^{18}O_{pr}$ correlation suggests this is possible using AH1, provided trends linked to other processes are removed.

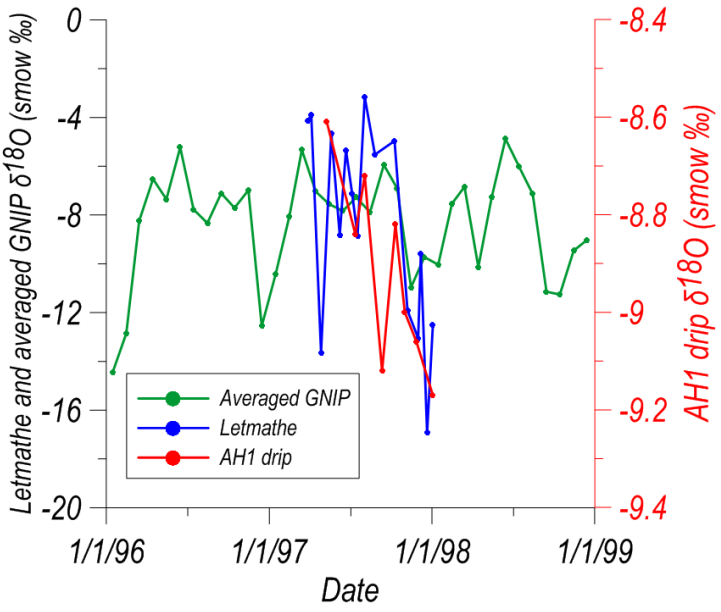

Figure 11 *- AH1 $\delta^{18}O_{dw}$ (red) compared to $\delta^{18}O_{pr}$ from the averaged GNIP data (green) and Letmathe (blue) [Niggemann (2001)].*

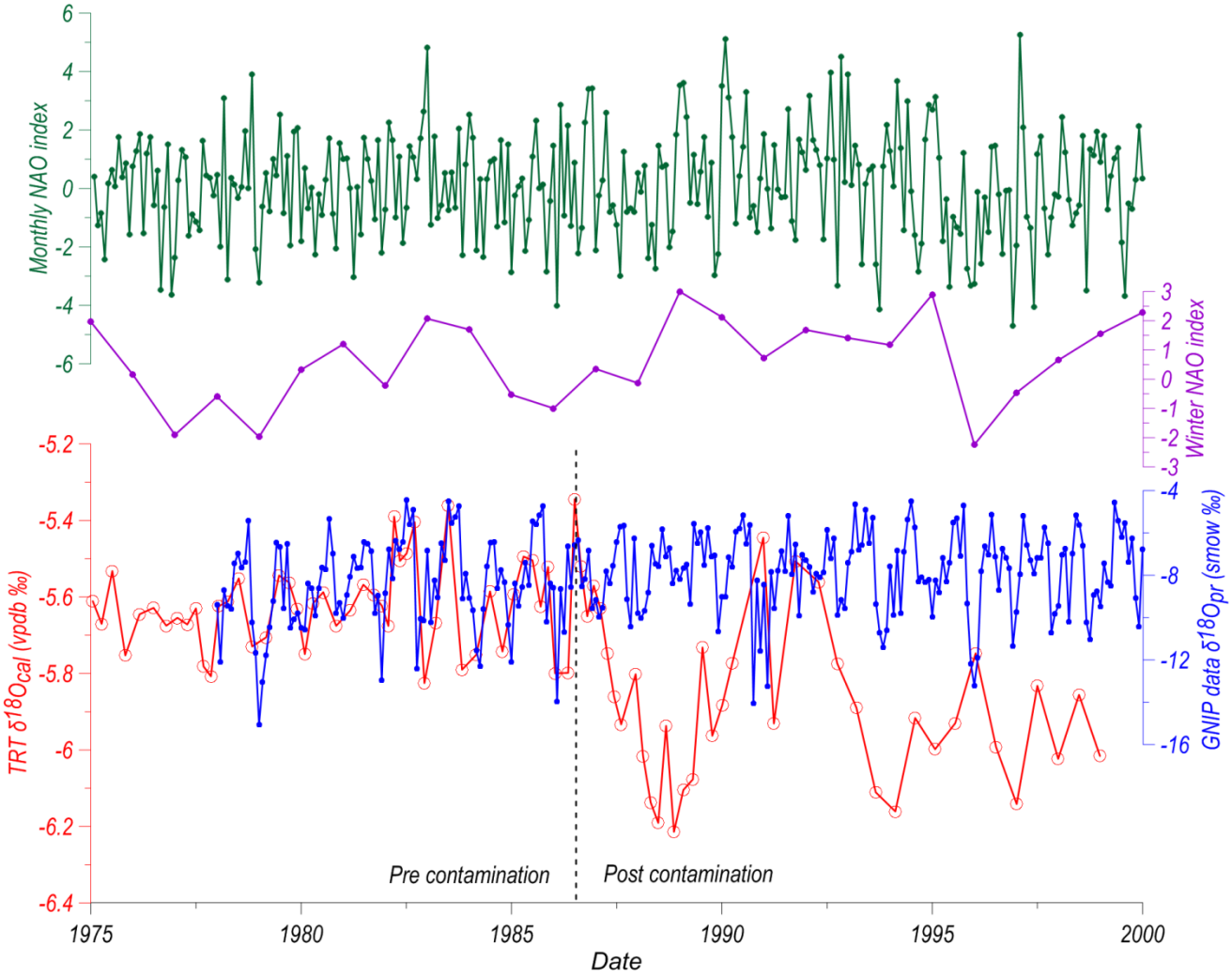

Figure 12 - *TRT $\delta^{18}O_{cal}$ (red), shifted by 1.5 years, compared to the averaged GNIP data $\delta^{18}O_{pr}$ (blue), the annual winter NAO index (purple) and the monthly NAO index (green).*

If annual winter NAO reconstruction was the goal, sampling a stalagmite with a higher growth rate than AH1, whilst maintaining high resolution micromilling, would provide the most potential. When choosing this stalagmite, drip water sensitivity to annual $\delta^{18}O_{pr}$ fluctuations also needs consideration. For example, a hypothetical stalagmite sampled at 25µm intervals that is highly sensitivity to annual $\delta^{18}O_{pr}$ fluctuations and has a growth rate of ~200µm/a, would provide excellent potential for reconstructing paleo $\delta^{18}O_{pr}$, and therefore winter NAO indices. Such a sample could be dated using annual $\delta^{18}O_{cal}$ cycles verified using the radiocarbon bomb spike, similar to this study. Further verification of the $\delta^{18}O_{pr}$ cycles could be established using trace element cycles, which are widely documented in stalagmites [Fairchild and Treble (2009)].

4 Conclusion

Reconstruction of winter North Atlantic Oscillation indices using $\delta^{18}O_{cal}$ values from central European stalagmites was investigated by very high resolution micromilling of a stalagmite (AH1) from northwestern Germany. The milled stalagmite powders were analysed with an IRMS in weight order, rather than sequentially. This highlighted the benefit of having a semi-random sample order when conducting drift corrections because a given sample's chemistry is independent of preceding and succeeding samples in terms of climatic processes, which allows instrumental drift to be identified and corrected with more certainty.

Cycles were identified in the $\delta^{18}O_{cal}$ data and, by counting cycles, a chronology was developed. Using the cycle count chronology, the radiocarbon bomb spike was accurately positioned, strongly suggesting that the cycles are annual and that the chronology is accurate. Hendy test results and precipitation and $\delta^{18}O_{dw}$ values suggest kinetic fractionation increased AH1's isotope ratios but the expression of annual cycles suggests it did not overprint the annual fluctuation in $\delta^{18}O_{pr}$.

The cycle count chronology indicates three key isotope excursions, which may be explained by historic cave events: i) the discovery of AH1's cave passageway in 1985 which led to contamination of the stalagmite, ii) clearing of vegetation above the cave during WWII, which may have resulted in increased isotope ratios possibly associated with decreased biogenic productivity and a shift in the summer/winter recharge distribution, and iii) the creation of the artificial entrance in 1925, which may have resulted in decreased kinetic fractionation associated with rerouted cave air flow and therefore decreased isotope ratios. However, apart from trace element data suggesting the discovery of AH1's cave passageway led to contamination of AH1 and a shift in

isotope ratios, these hypotheses are based on the coincidence of historical events and shifts in isotope ratios within AH1, so remain speculative.

A good visual correlation between GNIP data and the $\delta^{18}O_{cal}$ cycles was achieved within the errors of the chronology. However, a good winter $\delta^{18}O_{cal}$ – winter NAO correlation was elusive because winter $\delta^{18}O_{cal}$ values were only documented by two or fewer datapoints and the true winter $\delta^{18}O_{pr}$ signal was not obtained by averaging these points. Although this suggests annual winter NAO indices cannot be reconstructed using AH1, the good visual $\delta^{18}O_{cal}$ - $\delta^{18}O_{pr}$ correlation suggests AH1 will record prolonged shifts in the winter NAO state, provided trends associated with other processes are removed.

5 References

Baldini, J. U. L., McDermott, F., Baker, A., Baldini, L. M., D., Mattey, P., Railsback, L. B., 2005. Biomass effects on stalagmite growth and isotope ratios: A 20^{th} centuary analogue from Wiltshire, England. EPSL. 240, 486-494.

Baldini, L. M., McDermott,F., Foley, A. M., Baldini, J.U.L., 2008. Spatial variability in European winter precipitation δ^{18}O-NAO relationship: Implications for reconstructing NAO-mode climate variability in the Holocene. Geophyical Research Letters. 35, doi:10.1029/2007GL032027

Breitenbach ,S. F. M., Bernasconi, S. M., 2011. Carbon and oxygen isotope analysis of small carbonate samples (20 to 100µg) with a GasBench II preparation devise. Rapid Communications in Mass Spectrometry. 25, 1910-1914.

Cook ,E. R., D'Arrigo, R. D., Briffa ,K. R., 1998. A reconstruction of North Atlantic Oscillation using tree-ring chronologies from North America and Europe. The Holocene. 8, 9-17.

Cook ,E. R., D'Arrigo ,R. D., 2002. A Well Verified, Multiproxy Reconstruction of the Winter North Atlantic Oscillation Index since A.D. 1400. Journal of Climate. 15, 1754-1764.

D'Arrigo ,R.D., Seager, R., Smerdon ,J. E., LeGrande , A. N., 2011. The anomalous winter of 1783-1784: Was the Laki eruption of an analog of the 2009-2010 winter to blame? Geophysical Research Letters. 38, doi:10.1029/2011GL046696.

Fairchild, I .J., Treble, P. C., 2009. Trace elements in speleothems as recorders of environmental change. Quaternary Science Reveiw. 28, 449-468

Fairchild, I. J., Smith, C.L., Baker, A., Fuller, L., Spötl, C., Mattey, D., McDermott, F., E.I.M.F, 2006. Modification and preservation of environmenttal signals in speleothems. Earth-Science Reviews. 75, 105-153.

Genty, D., Vokal, B., Obelic, B., Massault, M., 1998. Bomb ^{14}C time history recorded in two modern stalagmites- importance for soil organic matter dynamics and bomb ^{14}C distribution over continents. EPSL. 160, 795-809.

Glueck, M.F., Stockton, C. W., 2001. Reconstruction of the North Atlantic Oscillation 1429-1983. International Journal of Climatology. 21, 1453-1465.

Goodkin, N. F., Hughen ,K. A., Doney, S. C., Curry, W. B., 2008. Increased multidecadal variability of the North Atlantic Oscillation since 1781. Nature Geoscience. 1, 844-848.

Hendy ,C.H., 1971. The isotopic geochemistry of speleothems-I. The calculation of the effecs of different modes of formation on isotopic composition of speleothems and their applicability as palaeoclimatic indicators. Geochimica et Cosmochimica Acta. 35, 801-824.

Hua, Q., Barbetti, M., 2004. Review of tropospheric bomb C-14 data for carbon cycle modelling and age calibration. Radiocarbon. 3, 1273-1298.

Hurrell, J. W., 1995. Decadal Trends in the North Atlantic Oscillation Regional Temperature and Precipitation. Science. 269, 676-679.

Hurrell, J. W., Kushnir, Y., Ottersen, G., Visbeck, M., 2003. An overview of the North Atlantic Oscillation. Geophysical Monograph. 134, 1-35.

Jackson, A. S., McDermott, F., Mangini, A., 2008. Late Holocene climate oscillations and solar fluctuations from speleothem STAL-AH-1, Sauerland, Germany: A numerical perspective. Geophysical Research Letters. 35, L06702

Jens Fohlmeister, University of Heidelberg (jens.fohlmeister@iup.uni-heidelberg.de)

Jones, P.D., Jonsson, T., Wheeler, D., 1997. Extension to the North Atlantic Oscillation using early instrumental pressure observations from Gibraltar and south-west Iceland. International Journal of Climatology. 17, 1433-1450.

Kim, S-T., O'Neil, J. R., 1997. Equilibrium and nonequilibrium oxygen isotope effects in synthetic carbonates. Geochemica et Cosmochimica Acta. 61, 3461-3475.

Langebroek, P. M., Werner, M., Lohmann, G., 2011. Climate information imprinted in oxygen-isotopic composition of precipitation in Europe. EPSL. 311, 144-154.

Luterbacher, J., Xoplaki, E., Dietrich, D., Rickli, R., Jacobeit, J., Beck, C., Gyalistras., D, Schmutz, C., Wanner, H., 2002. Reconstrcution of sea level pressure field over the Eastern North Atlantic and Europe back to 1500. Climate Dynamics. 18. 545-561.

Mattey, D., Lowry, B., Duffet, J., Fisher, R., Hodge, E., Frisia, S., 2008. A 53 year seasonally resolved oxygen and carbon isotope record from a modern Gibraltar speleothem: Reconstructed drip water and relationship to local precipitation. EPSL. 269, 80-95.

McDermott, F., 2004. Palaeo-climate reconstruction from stable isotope variations in speleothems: a review. Quaternary Science Reviews. 23, 901-918.

Meeker, L. D., Mayewski, P. A., 2002. A 1400-year high resolution record of atmospheric circulation over the North Atlantic and Asia. The Holocene. 12, 257-266.

www.metoemedia.de

Niggemann, S., Mangini, A., Mudelsee, M., Richter, D.K., Wurth, G., 2003. Sub-Milankovitch climatic cycles in Holocene stalagmites from Sauerland, Germany. EPSL. 216, 539-547.

Niggemann, S., Mangini, A., Richter, D.K., Wurth, G., 2003. A paleoclimate record of the last 17,600 years in stalagmites from the B7 cave, Sauerland, Germany. 22, 555-567.

Niggemann, S., 2000. Klimabezogene Untersuchungen an spät- bis postglazialen Stalagmiten aus Massenkalkhöhlen des Saurlandes. In: Richter, D.K. & Wurth, G. (Hrsg): Belräge zur Speläologie Bochumer geol. u. Geotechn. Ard., 5 5: 5-129; Bochum.

Raible, C. C., Yoshimori, M., Stocker, T.F., Casty, C., 2007. Extreme midlatitude cyclones are their implications for precipitation and wind speed extremes in simulations of the Maunder Minimum versus present day conditions. Climate Dynamics. 28, 409-423.

Riechelmann, D.F.C., Schröder-Ritzau, A., Scholz, D., Fohlmeister, J., Spötl, C., Richter, D.K., Mangini, A., 2011. Monitoring Bunker cave (NW Germanny): A prerequisite to interpret geochemical proxy data of speleothems from this site. Journal of Hydrology. 409, 682-695.

Seager, R., Kushnir, Y., Nakamura, J., Ting, M., Naik, N., (2010). Northern Hemisphere winter snow anomalies: ENSO, NAO and the winter of 2009/10. Geophysical Research Letters. 37, L14703

Shindell, D. T., Schmidt, G. A., Mann, M. E., , Rind, D., Waple, A., 2001. Solar Forcing of Regional Climate Change During the Maunder Minimum. Science. 294, 2149-2152.

Stuvier, M., Reimer, P.J., Braziunas, T.F., 1998. High precision radiocarbon age calibrations for terrestrial and marine samples. Radiocarbon, 40, 1127-111.

Tremaine, D. M., Froelich, P. N., Wang, Y., 2011. Speleothem calcite famred in situ: Modern calibration of $\delta^{18}O$ and $\delta^{13}C$ paleoclimate proxies in a continuously-montitored natural cave system. Geochemica et Cosmochimica Acta. 75, 4929-4950.

Trouet, V., Esper, J., Graham, N. E., Baker, A., Scourse, J. D., Frank, D. C., 2009. Persistent Positive North Atlantic Oscillation Mode Dominated the Medieval Climate Anomaly. Science. 324, 78- 80.

Trouet, V., Scourse, J.D., Raible, C.C., 2011. North Atlantic storminess and Atlantic Meridional Overturning Circulation during the last Millennium: Reconciling contradictory proxy records of NAO variability. Global Planetary Change. 84-85, 48-55.

Yan, H., Sun, L., Wang, Y., Huang, W., Qiu, S., Yang, C., 2011. A record of the Southern Oscillation Index for the past 2,000 years from precipitation proxies. Nature Geoscience. 4, 611-614.